Magnetic phase transitions in double hexagonal close packed neodymium metal-commensurate in two dimensions



1994 J. Phys.: Condens. Matter 6 5201

(http://iopscience.iop.org/0953-8984/6/27/029)

J. Phys.: Condens. Matter 6 (1994) 5201–5222. Printed in the UK

# Magnetic phase transitions in double hexagonal close packed neodymium metal—commensurate in two dimensions

B Lebech†, J Wolny‡ and R M Moon§

† Physics Department, Risø National Laboratory, Denmark

‡ Faculty of Physics and Nuclear Techniques, University of Mining and Metallurgy, Cracow, Poland

§ Solid State Division, Oak Ridge National Laboratory, Oak Ridge, TN, USA

**Abstract.** In elemental neodymium, a series of phase transitions between multi-$q$ modulated magnetic structures takes place below the magnetic ordering temperature $T_N$. Based on extensive neutron diffraction studies of the temperature dependence of the length and orientation of the modulation vectors associated with these structures we suggest that there exists a simple phenomenological relationship between the symmetry of the double hexagonal crystal lattice and the symmetry of the corresponding magnetic lattice. The model has a resemblance to the situation found for monolayer films on solid surfaces (orientational epitaxy) when considering the spin system as the adsorbate and the atomic structure as the substrate. In one dimension, the modulated magnetic structures are sequences of a commensurate to incommensurate transition followed by incommensurate to incommensurate transitions followed by an incommensurate to commensurate transition. However, in two dimensions, all the modulated magnetic structures are equally well described as higher-order commensurate to commensurate transitions, where the magnetic unit cell is commensurate with the crystallographic unit cell, but rotated by some angle around the hexagonal axis with respect to the crystallographic unit cell. The rotation angle as well as the magnetic unit cell depend on temperature. The data suggest that the rotation angle is zero whenever there is a change from one type of multi-$q$ structure to another, i.e., in this case, the magnetic and the crystallographic unit cells are commensurate in both one and two dimensions. Previous and recent results for the light rare earth metals neodymium and praseodymium and alloys thereof, which lend support to this interpretation, are reviewed.

## 1. Introduction

It is well known from the literature that the light rare earth metals neodymium and praseodymium crystallize in the double hexagonal close-packed crystal (DHCP) structure (Koehler 1972) with only minor differences in their lattice constants. The two elements form a complete range of solid solutions, which despite their identical crystal structure exhibit a variety of magnetic behaviour. Elemental Pr is a singlet ground state system, which orders in a basal plane modulated magnetic structure only at very low temperatures (well below 1 K) (McEwen and Stirling 1981, Møller *et al* 1982). Elemental Nd, on the other hand, is a Kramers doublet, which passes through a sequence of basal plane modulated magnetic structures below the Néel temperature $T_N = 19.9$ K (Moon *et al* 1964, Lebech 1981, McEwen *et al* 1985, Forgan *et al* 1989, 1992b, Gibbons *et al* 1992). The Nd rich alloys of Nd and Pr form magnetic structures that at high temperatures are similar to those found in Nd, and at low temperatures the experimental results indicate the existence of modulated structures with a $c$-axis commensurate component of the modulation vector both in Nd (Forgan *et al* 1992b) and in the Nd rich Nd–Pr alloys (McEwen *et al* 1986, Zochowski *et al* 1992, Wolny and Lebech 1995).

0953-8984/94/275201+22$19.50  

Before continuing, we review what is known about the magnetic structure in elemental Nd. Most of this knowledge is based on neutron diffraction data although other techniques, both theoretical and experimental, have also been essential. The crystal structure is hexagonal with a four-layer stacking sequence along the *c*-axis of the type ABAC. The atoms in the A layers have a nearly face centred cubic arrangement of nearest-neighbour atoms and are usually called the cubic sites. The atoms in the B and C layers have a hexagonal arrangement of nearest neighbours and are therefore called the hexagonal sites. Consequently, these two types of site may behave differently magnetically, as indeed experiments show they do. From the symmetry point of view the most important difference between the two sites is the inversion symmetry, which belongs to the symmetry elements of the cubic sites, but *not* to the symmetry elements of the hexagonal sites. Because of this property, the twofold axes in the basal plane for cubic sites are parallel to the three equivalent symmetry related directions given by the real space $\hat{a}_k$ vectors, whereas the twofold axes in the basal plane for hexagonal sites are parallel to the symmetry related reciprocal space $\hat{a}_k^*$-vectors (see figure 1). In this context, it is worth noticing that the $\hat{a}_k^*$-vectors are also parallel to the mirror planes perpendicular to the basal plane of the DHCP structure. Throughout the paper, we use $\hat{u}$ to signify a unit vector along $u$, square brackets to indicate directions of axes and angle brackets to indicate symmetry related directions, i.e. $[hkl]$ and $\langle hkl \rangle$, respectively.

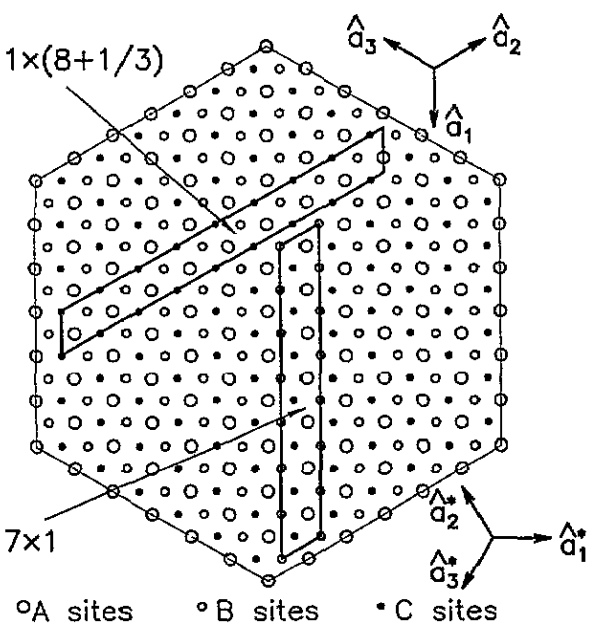


**Figure 1.** A projection of all atoms in the DHCP lattice on a single hexagonal plane. Cubic A sites are shown as o, hexagonal B and C sites as ○ and ●, respectively. The bold parallelograms indicate the $7 \times 1$ and $1 \times (8+\frac{1}{3})$ commensurate magnetic unit cells, respectively (see section 2). Also shown are the real ($\hat{a}_i, i = 1, 2, 3$) and the reciprocal lattice unit vectors ($\hat{a}_i^*, i = 1, 2, 3$).

The magnetic structure of Nd was first described by Moon *et al* (1964) as a single-$q$ modulated structure where the moment $\mu(r_i)$ at site $r_i$ in the magnetic domain $k$, is given

by

$$\mu(r_i) = \mu_k \cos(q_k \cdot r_i + \alpha_k) \qquad k = 1, 2 \text{ or } 3 \tag{1}$$

with $\mu_k$ and $q_k$ along the three equivalent reciprocal lattice vectors $\hat{a}_k^*$, i.e. perpendicular to the edges of the regular hexagon forming the crystal structure. As noted above, these directions have the highest symmetry in the basal plane for hexagonal sites and they also correspond to some of the symmetry elements for the cubic sites. It is therefore not surprising that in the first experiments, the basal plane modulation vectors forming the magnetic structure were found to be aligned along these directions. Moon *et al* (1964) also suggested that at high temperatures only the hexagonal sites ordered according to (1), whereas both sites were ordered in a similar way at lower temperatures, but with different modulation vectors associated with the ordering at each of the two sites.

In an attempt to explain certain discrepancies between the single-$q$ model predictions and the experimental findings it was suggested by Bak and Lebech (1978) that the structure was instead a so called three-$q$ structure where the moments modulated by the three symmetry related modulation vectors $q_k$ are coupled to give a resultant moment, $\mu(r_i)$ at site $r_i$, where

$$\mu(r_i) = \sum_{k=1}^{3} \mu_k \cos(q_k \cdot r_i + \alpha_k). \tag{2}$$

This structure is the vector sum of three modulated moment components $\mu_1(r_i)$, $\mu_2(r_i)$ and $\mu_3(r_i)$ of the same form as given by (1). The moment amplitudes and the modulation vectors of these three components form a three-armed star (see figure 2(a)) with 120° between the arms of the star. In (1) and (2), we have used the original notations of Bak and Lebech (1978), and it should be emphasized that the index $k$ has significantly different meanings in (1) and (2). In (1), the index $k$ refers to each of the possible magnetic domains that may be populated in a multi-domain single-$q$ magnetic structure with modulation vector along one of the symmetry related directions. In (2), the index $k$ refers to the moment components that by vector addition form the resulting moment at site $r_i$ in a single-domain three-$q$ structure with modulation vectors along the three symmetry related directions defined by the star of vectors $q$. For Nd, this means that (1) describes $\mu(r_i)$ for one of the six equivalent magnetic domains in the single-$q$ structure, while (2) describes $\mu(r_i)$ for one of the two equivalent magnetic domains in the three-$q$ structure. It is also worthwhile to note that in principle the summation over the index $k$ in (2) can take any value, in which case (2) describe the moment at site $r_i$ of a single domain of more general magnetic structures, the so called multi-$q$ structures. For these multi-$q$ structures, the number of possible magnetic domains will most often be larger than two.

When proposed for Nd, the three-$q$ model described by (2) was based on Landau symmetry arguments and renormalization group theory. One of the results of this treatment is that the magnetic order transition at $T_N$ is first order provided the order is to a single-$q$ magnetic structure, whilst the transition at $T_N$ is second order provided the order is to a three-$q$ magnetic structure. The then accepted experimental fact was that the magnetic ordering transition was of second order. Accordingly, this could only be consistent with a three-$q$ magnetic structure, and hence such a structure model was proposed for Nd. A further prediction of the three-$q$ model was that lattice modulations caused by spin–lattice couplings should accompany the onset of magnetic ordering. The existence of these modulations was not confirmed experimentally. Instead it was revealed (Moon *et al* 1979, Lebech *et al*

1979, Lebech and Als-Nielsen 1980) that at $T_2$ about 1 K below $T_N$, both $q_k$ and $\mu_k$ turn away from the high-symmetry $a_k^*$ directions. The angles between $a_j^*$ and $q_k$ or $a_j^*$ and $\mu_k$ are $\sim 2.5°$ or $\sim 15°$ (Lebech 1981), respectively. More recent measurements of lattice expansion in Nd by Zochowski *et al* (1986) showed unambiguously that the transition at $T_N$ is first order. Therefore, according to the theoretical predictions of Bak and Lebech (1978) the incipient magnetic order must be a single-$q$ structure as originally suggested by Moon *et al* (1964). However, this does not exclude transitions at lower temperatures to multi-$q$ magnetic structures similar to the three-$q$ structure described by (2). In fact McEwen *et al* (1985) have suggested and given experimental evidence that below $T_2$ the magnetic structure of Nd is a two-$q$ structure, where the angle between the two coupled moment components $\mu_k$ and $\mu_l$ is $\sim 90°$, and the angle between the corresponding modulation vectors $q_k$ and $q_l$ is $\leqslant 120°$ (figure (2(b)) in agreement with the findings of Lebech (1981). Based on a series of neutron diffraction studies in applied magnetic field or under pressure, McEwen, Forgan and collaborators (McEwen *et al* 1982, 1985, Forgan *et al* 1989, Zochowski *et al* 1991, Forgan *et al* 1992a, b, Forgan 1992, Gibbons *et al* 1992) have, in a very convincing way, proposed that below 10 K, the moments associated with the magnetic order on both crystallographic sites couple to form first a three-$q$ structure (figure 2(c)) and then, at even lower temperatures, a four-$q$ magnetic structure (figure 2(d)). All of these multi-$q$ magnetic structures may as mentioned earlier be described by generalization of (2).

Figure 2 gives an illustration of the different multi-$q$ structures observed in Nd. The right hand diagrams of figure 2 display the diffraction patterns observed around a particular reciprocal lattice point (*) in a multi-domain sample. The two left-hand diagrams show the relative orientations of the basal plane projections of the modulation vectors $\hat{q}_{ij}$ and the moment amplitudes $\hat{\mu}_{ij}$, where the index $i$ labels the moment component ($i \equiv 1$ for the single-$q$ structure) and the index $j$ labels the magnetic domain. This double labelling of the modulation vector and the moment component is used only in connection with figure 2 and the rest of this section in order to avoid the ambiguity of (1) and (2). The single-$q$ structure given by (1) and the three-$q$ structure given by (2) are in fact both illustrated in figure 2(a). In the single-$q$ case given by (1), $(\hat{q}_{11}, \hat{\mu}_{11})$, $(\hat{q}_{12}, \hat{\mu}_{12})$ and $(\hat{q}_{13}, \hat{\mu}_{13})$ refer to the sets of coupled modulation vectors and moment amplitudes for three of the symmetry related magnetic domains that may coexist in a multi-domain sample with hexagonal symmetry and modulation along a basal plane symmetry direction. In the three-$q$ case given by (2), $(\hat{q}_{11}, \hat{\mu}_{11}, \hat{q}_{21}, \hat{\mu}_{21}, \hat{q}_{31}, \hat{\mu}_{31})$ refer to one set of coupled modulation vectors and moment amplitudes for a single magnetic domain in a three-$q$ sample with hexagonal symmetry and modulations along basal plane symmetry directions. For both the single-$q$ three-domain and the three-$q$ one-domain cases, all six diffraction spots shown on the right hand side of figure 2(a) have the same intensity when disregarding geometrical factors. The filled circles arise from the $(\hat{q}_{11}, \hat{\mu}_{11})$ (or $(-\hat{q}_{11}, -\hat{\mu}_{11})$) magnetic domains shown by thick arrows on the left in figure 2(a), while the unfilled circles arise from the remaining symmetry related magnetic domains. Although the right hand side of figure 2(a) displays the diffraction pattern for the single-$q$ case, it may also illustrate the intensity pattern for three-$q$ case given by (2) with modulation vectors and moments given by $(\hat{q}_{11}, \hat{\mu}_{11}, \hat{q}_{21}, \hat{\mu}_{21}, \hat{q}_{31}, \hat{\mu}_{31})$ and shown by thick and dot-dashed arrows and by the letters in parenthesis in figure 2(a). In this case, all the diffraction spots would have to be shown as filled circles.

In figure 2(b), (c) and (d), which illustrates the special two-$q$, three-$q$ and four-$q$ magnetic structures observed below $T_2$ in Nd, only one set of coupled modulation vectors and moment amplitudes (one domain, $j \equiv 1$) is shown, even though we most often consider a group of diffraction spots originating from different magnetic domains. As mentioned previously, the diffraction patterns on the right of figure 2 show all the diffraction spots

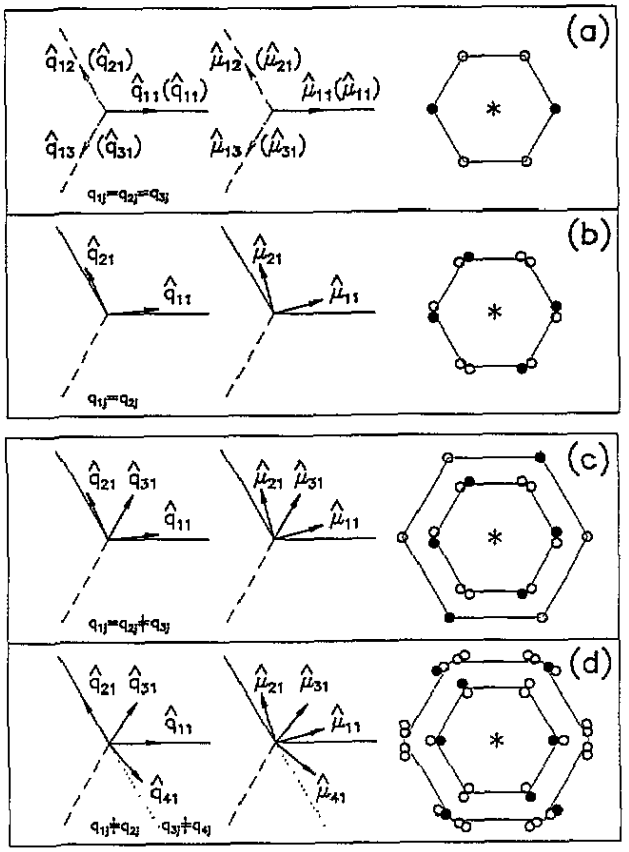


**Figure 2.** Directions of the basal plane projections of the modulation vectors, moment amplitudes and the corresponding diffraction patterns around a particular nuclear Bragg point (*) for the multi-$q$ structures described in the text. For illustrative purposes, the angles between the symmetry directions and the $\hat{q}$-vectors are doubled and the angles between the coupled moments $(\hat{\mu}_{ij}, \hat{\mu}_{2j})$ and $(\hat{\mu}_{3j}, \hat{\mu}_{4j})$ are identical to 90°. The indices $i$ and $j$ used for $\hat{q}$ and $\hat{\mu}$ refer to the coupled $\hat{q}$- and $\hat{\mu}$-vectors and to the domain label, respectively.

that may be observed in a multi-domain sample. The filled circles arise from the domain corresponding to the coupled modulation vectors and moment amplitudes shown by the thick arrows on the left in figure 2(b), (c) and (d), while the unfilled circles arise from the remaining symmetry related magnetic domains. It should be emphasized that in general each group of magnetic satellites (for instance the left hand group of four satellites in figure 2(d)) will originate from different magnetic domains. It should further be noted that figure 2(c) shows a special case of the three-$q$ structure with $\hat{q}_{31}$ parallel to the [010] direction. If, instead, $\hat{q}_{31}$ is rotated slightly with respect to the [010] direction, the corresponding satellites will split in a similar way to the $q_{11}$ and $q_{21}$ satellites (see for instance figure 2(b)), and the number of satellites around the Bragg point will be increased by six.

## 2. Description of one-dimensional commensurate–incommensurate phase transitions in Nd

In the following we shall not be concerned with which type of multi-$q$ structure describes

the magnetic structure of Nd in a particular temperature range. We shall concern ourselves only with the temperature dependence of the length and direction of the modulation vector and attempt to explain some common features of the magnetic ordering of the Nd and Nd–Pr alloys in terms of the symmetry of the DHCP crystal structure.

Before continuing, we need to define what we mean by one-dimensional commensurate or incommensurate magnetic phase transitions in Nd. For any basal plane modulated structure we may write

$$q = (q_x, q_y) \tag{3}$$

where $q_x$ and $q_y$ are the Cartesian coordinates of $q$ in units of $|a^*|$. For $q$ along the direction of highest symmetry for the hexagonal sites, $q_y \equiv 0$, and the structure is commensurate *only* if $q_x$ is given by rational numbers. The fundamental commensurate values are therefore given by the following relations:

$$q_x = 1/n \qquad q_y = 0 \tag{4}$$

where $n$ is an integer. One-dimensional commensurate–incommensurate phase transitions for the modulation vectors associated with order for instance at the hexagonal sites will be given by deviations from (4), for instance by $q_y \neq 0$.

If we consider the basal plane projection of figure 1, it is obvious that there is a shift of

$$\pm \tfrac{1}{3}(2\pi/a^*) \tag{5}$$

between the hexagonal and the cubic sites along the $\hat{a}^*$ direction, and when, at low temperatures, the cubic and hexagonal sites start to interact, we may expect the following relations to describe the fundamental commensurate values of the basal plane components of the modulation vector rather than the relations given by (4):

$$q_x = 1/(n \pm \tfrac{1}{3}) \qquad q_y = 0. \tag{6}$$

Here, $n$ is an integer assumed in (4). However, in principle $n$ may even be a fractional number, in which case (4) and (6) describe higher-order commensurate structures.

Equations (4) and (6) describe two different situations for the one-dimensional commensurate structures: (4) is fulfilled when the modulation originates from interaction between atoms within a single basal plane (of either hexagonal or cubic site atoms) perpendicular to the $c$-axis. Equation (6) is fulfilled when the interaction between sites belonging to near-neighbour planes (cubic and hexagonal) starts to dominate. It should be emphasized that if we consider the spin system as the adsorbate and the atomic structure as the substrate, the conditions given by (4) and (6) are equivalent to the situation reported for monolayer films on solid surfaces, i.e. orientational epitaxy. Whenever the structure of the material adsorbed on a homogeneous substrate becomes incommensurate with the substrate, the lattice formed by the adsorbed atoms is twisted in relation to the substrate lattice. The ground state for these systems is the incommensurate solid with static distortion waves that has been treated theoretically by Novaco and McTague (1977), Shiba (1980), Grey and Bohr (1991) and Bohr and Grey (1992).

When illustrating our ideas in relation to the behaviour of the modulation vector in Nd and Nd–Pr alloys we assume that there is competition betwen the crystalline substrate favouring an orientational epitaxial arrangement of the spins on the hexagonal plane substrate and the oscillatory nature of the magnetic interactions between neighbouring spins. Let us

now consider how this could agree with the results of the neutron diffraction studies. For Nd the neutron diffraction studies show that near $T_N$, where the magnetic interactions are relatively weak, only the hexagonal sites order magnetically with moments and modulation vectors confined to a single hexagonal plane. If we assume that the crystal structure dominates the formation of the incipient magnetic order, a commensurate modulated magnetic structure would be described by an in plane modulation vector that connects hexagonal sites only, i.e. the structure would be commensurate if (4) is obeyed. In figure 1 we illustrate this by the $7 \times 1$ magnetic unit cell, which corresponds to $n = 7$. Within the accuracy of the presently available experimental data this agrees reasonably well with the $q(T_2)$ for Nd (see figure 7), and for $Nd_{0.75}Pr_{0.25}$ and $Nd_{0.65}Pr_{0.35}$ (Wolny and Lebech 1995).

As the temperature is lowered the magnetic interactions grow, and at some temperature the order on the hexagonal sites induces a moment on the cubic sites. If we limit the discussion to only the in plane commensurate component of the modulation it must be a vector parallel to a high-symmetry direction that connects a hexagonal site to a cubic site in the nearest cubic layer, i.e. for the magnetic structure to be commensurate (6) should be obeyed. This is also illustrated in figure 1, where the $1 \times (8 + \frac{1}{3})$ magnetic unit cell corresponds to $(q_x, q_y) = (\frac{3}{25}, 0)$. At even lower temperatures we may further have magnetic structures for which the order is dominated by interactions between cubic sites only, i.e. a commensurate structure may once again be given by (4), similar to the case illustrated by the $7 \times 1$ unit cell shown in figure 1. Experiments show that one could even envisage a situation where the cubic site moments become large enough to induce additional order on the hexagonal sites, i.e. (6) is again valid.

## 3. Summary of experimental evidence for commensurate–incommensurate transitions in Nd

### *3.1. Description of the effects of experimental resolution*

Before correlating these ideas to the observed temperature behaviour of the modulation vectors in Nd we need to consider briefly the experimental arrangement and the effect of the instrumental resolution on the observed diffraction patterns. The data to be presented below are from measurements on two different Nd single crystals performed at different neutron spectrometers, in different sample environments and at different reactors. The data sets are qualitatively consistent, and illustrate fully the complex behaviour of the magnetic structures of Nd. The single-crystal samples were oriented either with a [−120] or the [001] axis vertical and perpendicular to the horizontal scattering plane. The diffractometers were either triple-axis instruments operating in the elastic mode, which allowed us to study only reflections in the horizontal plane, or a two-axis diffractometer with a detector that could be tilted out of the horizontal plane (normal beam inclination geometry). This latter instrument allowed us to study reflections both in and above the horizontal plane (higher layers), which as we shall see below was rather essential.

Figure 3 illustrates the horizontal plane projections of Bragg spots and corresponding resolution ellipses for two closely spaced satellite reflections (filled circles) in a hexagonal arrangement perpendicual to [001] around a general reciprocal lattice point (*hkl*) (unfilled circles). Figure 3(a)–(d) shows the situation for crystal orientation I ([001] direction perpendicular to the plane of the figure) for satellites split along $q_y$ (figure 3(a) and (c)) or for satellites split along $q_x$ (figure 3(b) and (d)). Figure 3(e) and (f) shows the equivalent situations for crystal orientation II ([−120] direction perpendicular to the plane of the figure). Here, and in the following, we refer the positions of the magnetic satellite reflections to

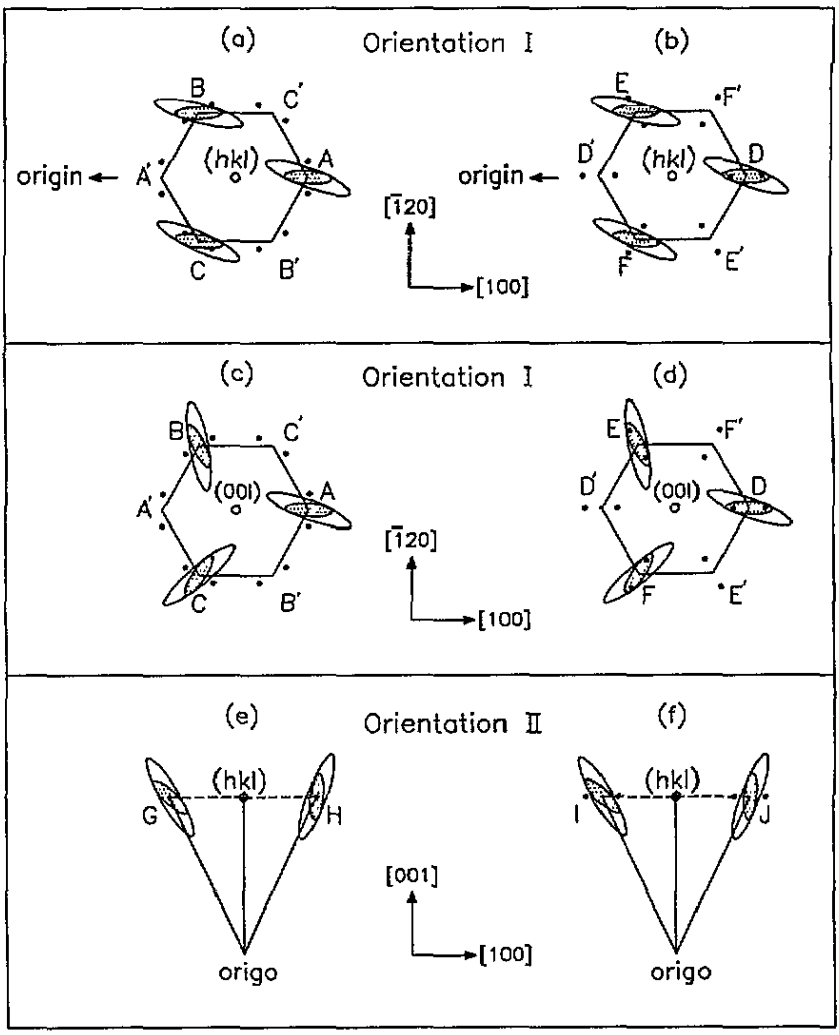


**Figure 3.** An illustration of the horizontal plane projections of the resolution ellipses with respect to the diffraction patterns observed in Nd for two different crystal orientations. For crystal orientation I, the [001] direction is perpendicular to the plane of the figure and for crystal orientation II, the $[-120]$ direction is perpendicular to the plane of the figure. (a), (c) and (e) are for satellites split in the $y$-directions ($q_y \neq 0$) and (d) and (f) are for satellites split in the $x$-directions ($q_{1x} - q_{2x} \neq 0$). The ellipses mark the half intensity contours. For clarity, the ellipses are enlarged with respect to the reciprocal lattice. The outer ellipses and the inner hatched ellipses correspond to relaxed and improved exit collimation, respectively. The unfilled circles are the reciprocal lattice point ($hkl$) and the filled circles the magnetic satellites. In general, the projection of the origin of the reciprocal lattice is far to the left in (a) and (b) as indicated by the arrows pointing to the left. Only for satellites around ($00l$) type nuclear reflections ((c) and (d)) does the origin of the reciprocal lattice project on top of the nuclear lattice position, resulting in identical orientation of ellipses for all satellite pairs.

Cartesian coordinate systems centred at the reciprocal lattice point ($hkl$). However, the ($x$, $y$)-axes for a particular set of satellites are oriented so that the $q_x$-directions always correspond to the directions of the symmetry related [100] reciprocal lattice directions.

For elastic scattering and relaxed exit collimation (unfilled ellipses), the angle between the reciprocal lattice vector and the long axis of the resolution ellipse will be approximately equal to the Bragg angle $\theta$ (Lebech and Nielsen 1975). When the exit collimation is improved, either by Soller slits or by means of an analyser crystal, the long axis shortens and the ellipse turns somewhat (hatched ellipses). It should be noted that, for a general lattice point ($hkl$), the projection (on the plane of the figure) of the origin of the reicprocal lattice lies far to the left in figures 3(a) and (b) as indicated by the arrows pointing to the left. This implies that from a resolution point of view the three satellite pairs (A, B and C or D, E and F) will generally be different as illustrated in figures 3(a) and (b). Only for satellites around (00$l$) (figures 3(c) and (d)), which may be studied in orientation I by tilting the detector out of the horizontal plane, does the origin project on top of the (00$l$) reciprocal lattice point. This further implies that, for (00$l$) type reflections, the resolution ellipses are identical by symmetry for all satellites surrounding the (00$l$) reciprocal lattice points, as illustrated for instance for the A, B and C or D, E and F satellites in figure 3(c) and (d). The above means that in general only some of the satellite pairs may be resolved. For this particular crystal orientation (orientation I) and an arbitrary reciprocal lattice point ($hkl$) (except (00$l$)), we have the following situation: satellites at A, A′ and F, F′ are well resolved, satellites at B, B′ and E, E′ are reasonably resolved and satellites at C, C′ and D, D′ are poorly resolved or unresolved. For satellites around (00$l$) the situation is as follows: all satellites are equivalent by symmetry, i.e. satellites corresponding to figure 3(c) ($q_y$ split) are all well resolved while satellites corresponding to figure 3(d) ($q_x$ split) are poorly resolved or unresolved.

As mentioned above, figure 3(e) and (f) shows the orientation of the resolution ellipses when the crystal is oriented with [−120] perpendicular to the plane of the figure. If ($hkl$) = (00$l$), the poor vertical resolution (perpendicular to the plane of the figure) causes satellites split by $q_y \neq 0$ (perpendicular to the plane of the figure) to appear as a single diffraction spot (figure 3(e)), while satellites split along $q_x$ will be extremely well resolved (figure 3(f)). For completeness, it might also be noted that if ($hkl$) = ($h$00) in figure 3(e), G and H correspond to the ($h0 \neq l$) nuclear Bragg points, respectively.

### *3.2. Results of the initial neutron diffraction studies*

The results of the initial neutron diffraction studies are shown in figures 4–6. In figure 4 we concentrate on the temperature region close to $T_N$. The figure shows the transition from the single-$q$ state (figure 2(a)), which appears at $T_N$, to the two-$q$ state (figure 2(b)), which starts to develop at $T_2 \sim 19.1$ K. The measurements were obtained using the HB-1 polarized beam triple-axis spectrometer at the high-flux isotope reactor at Oak Ridge National Laboratory, USA. The single-crystal sample was approximately cubic in shape (4 mm along an edge) and weighed 0.469 g. It is identical to the one used by Moon *et al* (1979), Moon and Koehler (1980) and Moon *et al* (1983). The sample was mounted with a [001] axis vertical (orientation I) in a variable-temperatue cryostat. The incident neutron wavelength was 2.44 Å, and the spectrometer was operating in the elastic mode with pyrolytic graphite monochromator and analyser crystals. The experimental set-up allowed us to study the magnetic satellites around the (100) nuclear Bragg peak. The resolution geometry corresponds to the situation depicted in figure 3(a) with improved exit collimation (hatched ellipses). Figure 4(a) and (b) shows neutron diffraction scans through the $(1 - q_x 00)$ (A′ in figure 3(a)) and $(1 - q_x q_x 0)$ (B in figure 3(a)) reciprocal lattice points in the $q_y$ direction with $q_x \sim \frac{1}{7}$. The solid curves are resoltion limited Gaussian fits. Above $\sim 19.1$ K the magnetic scattering at $(1 - q_x 00)$ (or $(1 + q_x 00)$) has vanished and the diffraction pattern at $(1 - q_x q_x 0)$ may equally well be fitted to a single peak broadened by

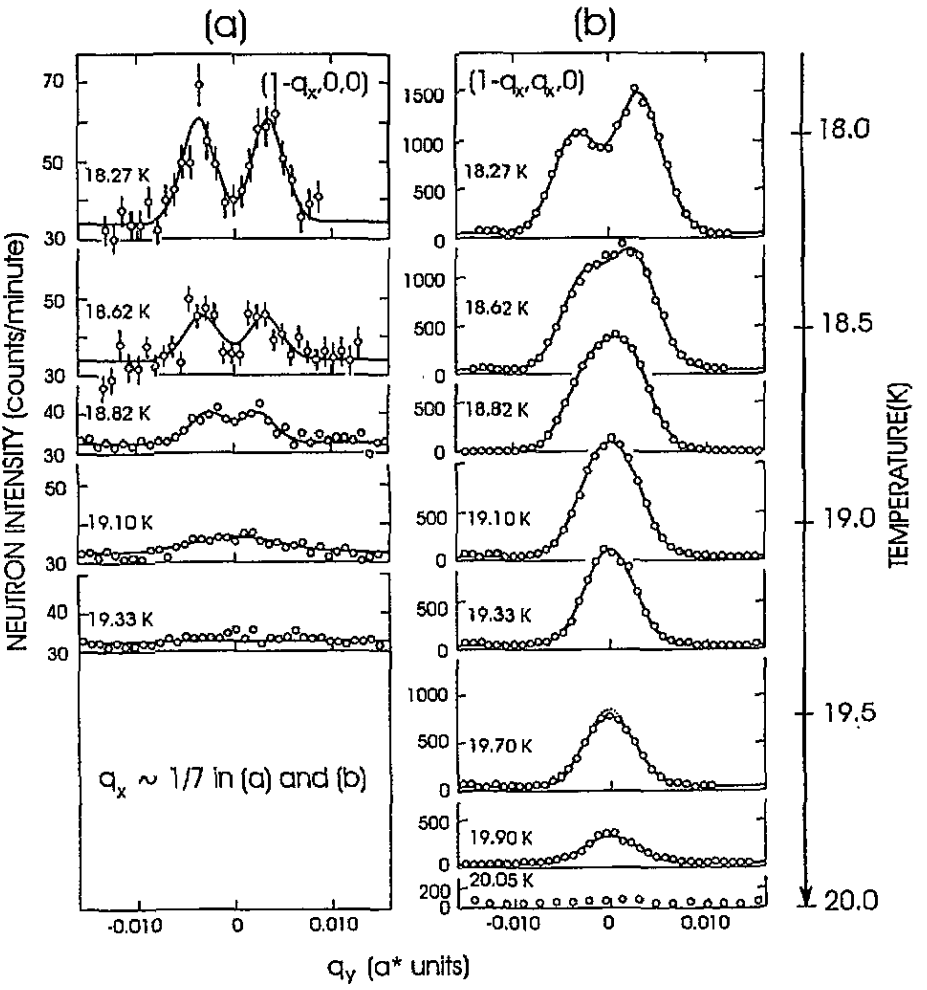


**Figure 4.** The temperature evolution of the magnetic satellites near the (100) reciprocal lattice point measured on heating. The data show the transition from the single-$q$ state near $T_N$ to the two-$q$ state appearing below $T_2 \sim 19.1$ K (see also figure 2(a) and (b)). The data obtained at the different temperatures are displaced by $\Delta T$ with respect to each other so that the ordinate values 30 and 0 coincide with the temperature scale to the right.

critical scattering (shown by dots for 19.7 K). The intensity difference between the satellite pair at $(1-q_x q_x 0)$ can be accounted for by geometrical factors in the magnetic cross section; it is not an effect of inhomogeneous domain population. The peaks around $(1-q_x 00)$ (or $(1+q_x 00)$) are weak and rather broad, and based only on the neutron diffraction data; it is *difficult to estimate accurately the transition temperature $T_2$ exactly. However,* $T_2 = 19.1$ K obtained from the measurements of thermal expansion (Zochowski and McEwen 1986) is consistent with the neutron diffraction data.

The data in figures 5 and 6 cover a wider temperature range, and illustrate the transitions from the two-$q$ state (figure 2(b)) via the three-$q$ (figure 2(c)) to the four-$q$ (figure 2(d)) states. Here, the data were obtained at the DR3 10 MW heavy-water moderated reactor at Risø National Laboratory, Denmark using either a thermal- or cold-neutron two-axis

diffractometer with a detector that could be tilted out of the horizontal plane (normal beam inclination geometry). The sample was a rectangular slab of dimensions $4 \times 4 \times 0.5$ mm$^3$. It is identical to the one used by Lebech *et al* (1979) and Lebech (1981). The crystal was mounted in a variable-temperature cryostat with the [001] axis vertical (orientation I). The incident neutron wavelength was 1.85 Å selected by the (111) reflection from a germanium monochromator. The tilting detector allowed high-resolution studies of magnetic satellites around the (00$l$) as well as around the (100) reciprocal lattice point, i.e. for tilt $> 0$ and tilt $= 0$, respectively.

Figure 5 shows data obtained close to the $(q_x 01)$ reciprocal lattice point at various temperatures below $T_N$. The figure shows equal-intensity contours (arbitrary scale) obtained by step scanning parallel to $q_y$ (the [−120] direction) in a net around $(q_x 01)$; figure 5(a) is for relaxed exit collimation and figure 5(c) for improved exit collimation. Above 19.1 K, figure 5(c) shows a single satellite originating from one of the domains of the single-$q$ state (figure 2(a)) with $|q| = |q_1| = q_1$. In the intermediate-temperature region above 10 K, figure 5(a) and (c) shows two peaks, which originate from two different domains in the two-$q$ state (figure 2(b)) with $|q_1| = |q_2|$. Between $\sim 8$ and $\sim 6$ K, the three satellites originate from threee different domains in the three-$q$ state (figure 2(c)) with $|q_1| = |q_2 \neq |q_3|$. Finally, below $\sim 6$ K, the three observed satellites originate from four different domains in the four-$q$ state (figure 2(d)) with $|q_1| \neq |q_2| \neq |q_3| \neq |q_4|$, where the satellite pair corresponding to $q_1$ and $q_2$ ($q_{1x} \sim 0.107$, $q_{2x} \sim 0.115$) is unresolved. It should be noted that in contrast to Forgan *et al* (1989), we find that even at 1.8 K, $q_{3x} = q_{4x} \sim 0.187$ for the $q_3$ and $q_4$ satellite pairs. However, the values for $q_y$ ($q_{3y} \sim 0.0125$ and $q_{4y} \sim 0.0195$) agree well with the data of Forgan *et al* (1989).

Figure 6 shows data obtained around the (100) reciprocal lattice point at 4.2, 10 and 16 K. The data give experimental evidence for the $q_x$ splitting of the $q_1$, $q_2$ satellites at low temperatures. In terms of resolution, the experimental set-up is the same as that used for figure 5(c). At 4.2 K (figure 6(a)), the resolution geometry corresponds to the situation depicted in figure 3(b), whereas the resolution geometry matches the situation depicted in figure 3(a) at 10 K (figure 6(b)) and 16 K (figure 6(c)). By comparing the equal-intensity contours at $(1 - q_x 0)$ at 16 and 4.2 K it is evident that at 4.2 K, the satellites are split along the $q_x$ direction and that $q_y = 0$. The same conclusion may be reached by comparing the satellites close to $(1 + q_x - q_x 0)$, but for these satellites the resolution in the $q_x$ direction is poorer and the conclusion is therefore not quite so obvious (see also figure 2 of the article by Lebech and als-Nielsen (1980)), but it has been confirmed by several neutron diffraction experiments. The equal-intensity contours in figure 6(b) and (c) are in full agreement with high-temperature data shown in figures 4 and 5, i.e. for $q_y \neq 0$.

### *3.3. Results of the final neutron diffraction studies*

Inspired by the experimental evidence presented in figures 4–6 in conjunction with the work by McEwen, Forgan and collaborators we made an extensive and systematic study of the temperature dependence of the lengths of the modulation vectors characteristic of the magnetic structures in Nd. From the previous studies (figures 4–6 and references given above) it had become obvious that not only systematic errors, but also the thermal hysteresis, caused significant problems when trying to correlate the lengths, $|q|$, of the modulation vectors derived by the different experimental groups and on different single-crystal samples. Although the above mentioned results on $q = (q_x, q_y)$ are qualitatively similar, they are not totally consistent. In order to obtain consistent data, a substantial data set was collected and the resulting temperature dependences of $q_x$ and $q_y$ are summarized in figures 7 and

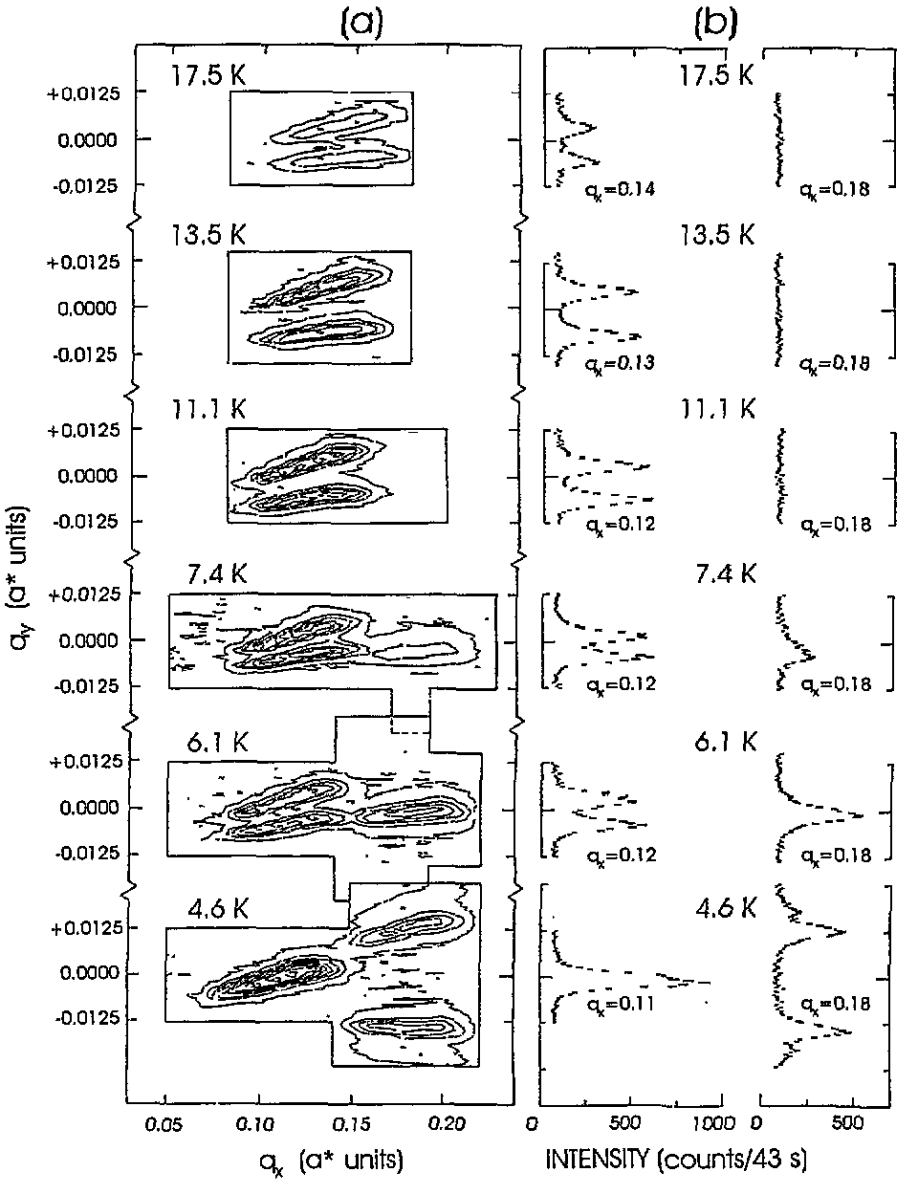


**Figure 5.** A summary of neutron diffraction data observed at different temperatures showing the magnetic Bragg peaks corresponding to $q_1$, $q_2$, $q_3$ and $q_4$ (see also figure 2). The figure shows equal-intensity contours (arbtrary scale) obtained by step scanning along $q_y$ in a net around $(q_x 01)$. (a) is for relaxed exit collimation and (c) for improved exit collimation. As examples, (b) and (d) show the corresponding intensity profiles obtained at relevant values of $q_x$ (see also figure 4). The polygons in (a) and (c) show the region of reciprocal space covered by the step scans.

8. These measurements were made at Risø National Laboratory using a cold-neutron two-axis diffractometer with a tilting detector (normal beam inclination geometry) as described earlier. The incident neutron wavelength was 2.39 Å, selected by a pyrolytic graphite monochromator crystal. We used the same single-crystal slab of Nd as used for the data

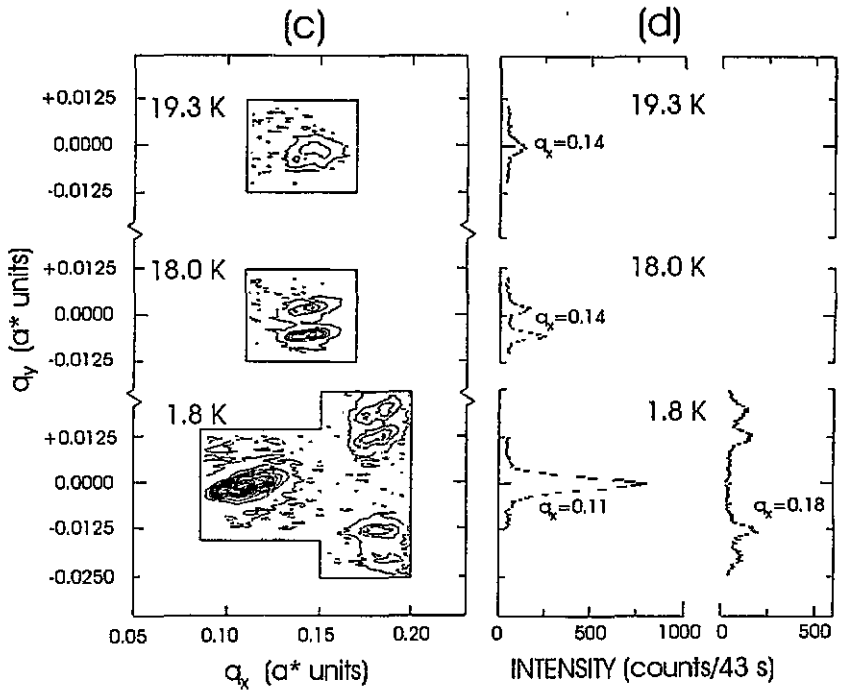


**Figure 5.** (Continued)

shown in figures 5 and 6. At the start of the measurements, the mosaicity was about 20′. However, possibly because of oxidation or the repeated thermal cycling, the crystal quality deteriorated and eventually the mosaicity became so large that the split satellites could no longer be resolved. Therefore, the data are less complete below 4.2 K, and some of our conclusions need to be further supported when new crystals become available.

The thermal hysteresis was considerable as illustrated for instance in the inset in figure 7(b), and special considerations were needed in order to establish the thermal history of the sample. Extreme care was therefore taken during thermal cycling. Before cooling, the sample was heated to 25 K and kept there for several minutes. Before heating, the sample was cooled to 4.2 K (or 1.8 K) and kept there for several minutes. In order to establish a reliable length scale, the lattice parameter was monitored at regular temperature intervals on both heating and cooling. In addition, both $q_x$ and $q_y$ were determined from the distances between pairs of satellites and scaled to the length of the (100) reciprocal lattice vector.

The crystal was mounted either with the [001] axis vertical (orientation I, figure 3(a) and (d)) or with the [−120] axis vertical (orientation II, figures 3(e)–(f)) in order to obtain the best possible resolution for the particular aspect of the modulation vector studied. In general, $q_x$ was determined from $\omega$-scans through (001) and (003) with the crystal in orientation II. The resolution configurations then correspond to figures 3(e) or (f) for satellites split in the $q_y$ directions ($q_1$ at high temperatures and $q_3(q_4)$ at low temperatures) and for satellites split along $q_x$ ($q_1$ and $q_2$ at low temperatures), respectively. $q_y$ was determined from $\omega$-scans through $(0q_x1)$ or $(0q_x3)$ with the crystal in orientation I, while $q_x$ was simultaneously monitored by scans parallel to the [100] direction with tilt> 0 from $(-q_x01)$ to $(q_x01)$. It should be emphasized that for the crystal orientation II (figure 3(e) and (f)), the tilting

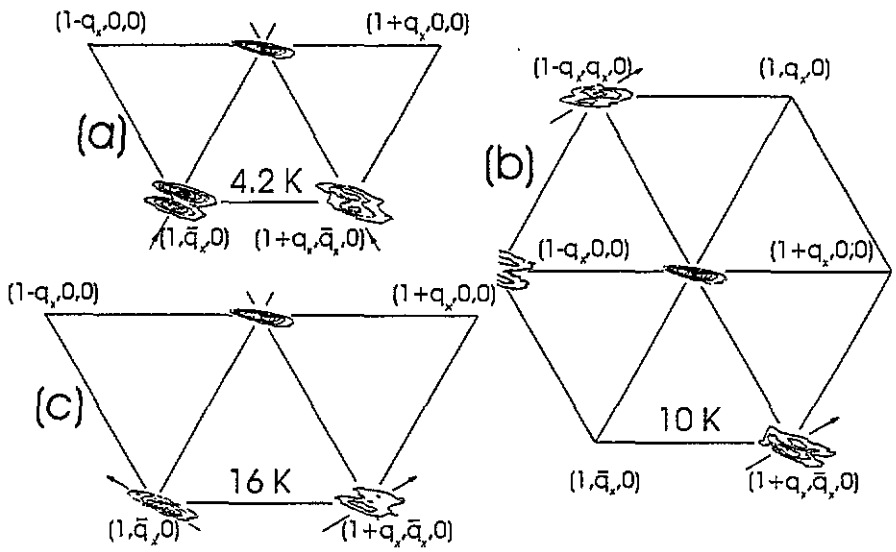


**Figure 6.** A summary of neutron diffraction data at 4.2, 10 and 16 K observed at different satellite positions around (100). The figure shows equal-intensity contours (arbitrary scale) obtained by step scanning along $q_y$ in a net around the particular satellite region with improved exit collimation. At 10 K, the off axis satellites $(1 \pm q_x \mp q_x 0)$ are about ten times less intense than the (100) nuclear peak, and they are about ten times more intense than the $(1 \pm q_x 00)$ satellites. The reason for the different satellite intensities is that only $\mu_y$ contributes to the $(1 \pm q_x 00)$ satellite intensities, while both $\mu_x$ and $\mu_y$ contribute to the off axis satellite intensities (see for instance Moon *et al* 1979).

detector arm offered extreme resolution along $q_x$ for $(00l)$ type reflections, in particular for $l = 1$, the reason for this being that, to a first approximation, the width of an $\omega$-scan is proportional to the detector set angle $\Gamma$. For the normal beam inclination geometry used here, $\Gamma$ and $\nu$ correspond to rotating the detector around a vertical and horizontal axis (detector tilt), respectively, and these angular settings define the scattering angle $2\theta_B$ through the relation $\cos(2\theta_B) = \cos(\Gamma)\cos(\nu)$. For $(00l)$ type satellite reflections, $\Gamma < 2\theta_B$, because $\nu \neq 0$. For the (001) satellites, we are in the small-angle limit ($\Gamma \simeq 0$), which means that the long axis of the resolution ellipse is almost perpendicular to the $q_x$-direction (figures 3(e) and (f)). Therefore, $q_x$ split magnetic satellites at I and J are very well resolved by $\omega$-scan or the nearly equivalent rock scans from I to J through (001). Similarly, although $q_y$ split satellites appear as one peak, the lengths of $q_x$ are accurately determined by $\omega$-scan or the nearly equivalent rock scans from G to H through (001).

The resulting data for $q_i = (q_{ix}, q_{iy})$ ($i = 1$ or 3) are summarized in figure 7, which shows the basal plane components of the modulation vectors in units of the (100) reciprocal lattice vector, where $q_1$ refers to the incipient modulation and $q_3$ refers to the additional modulation appearing below $\sim 8$ K. The thermal hysteresis is evident and may account for the relatively large differences between the lengths of the magnetic modulation vectors in Nd that are quoted in the literature. For completeness, the values of $q_y$ determined from the data obtained at Oak Ridge National Laboratory (figure 4) are shown as unfilled triangles in figure 7(c). Despite the facts that these data are neither measured on the same crystal nor in the cryostat as the rest of the data shown in figure 7(c) and the thermal history is not so well established, the two data sets agree remarkably well and illustrate the lock in $(q_y = 0)$ at $T \sim 19.1$ K or $q_x \sim \frac{1}{7}$.

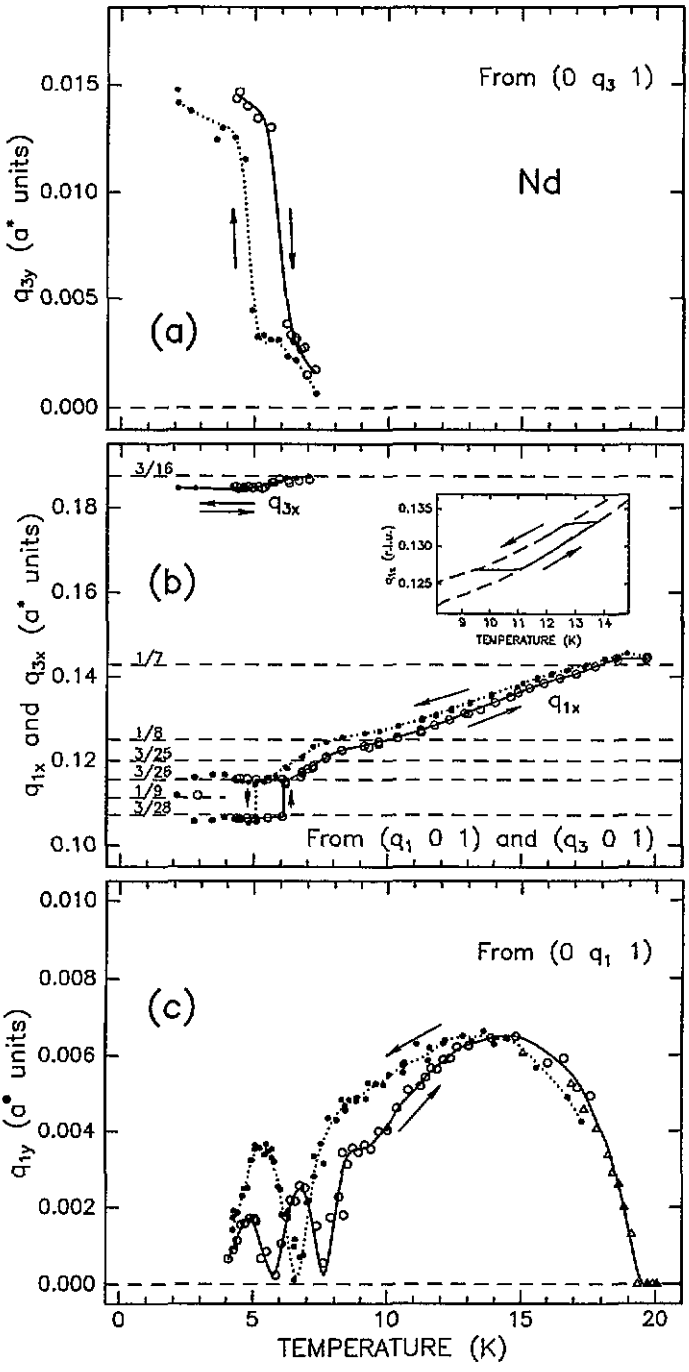


**Figure 7.** Temperature dependences of the basal plane components of the modulation vectors $q_1(q_{1x}(T_N) \sim \frac{1}{7})$ and $q_3(q_{3x}(T) \sim \frac{3}{16})$. (a) shows the $q_{3y}$ component, (b) the $q_{1x}$, $q_{2x}$ and $q_{3x}$ components and (c) the $q_{1y}$ component. The full and dotted curves are guides to the eye. Filled and unfilled circles correspond to cooling and heating, respectively. The inset in (b) shows, as an example of the pronounced thermal hysteresis, the loop followed by $q_{1x}$ after cooling from $T_N$ to $\sim 9$ K and heating to $\sim 14$ K followed by repeated cooling. The unfilled triangles in (c) are derived from the data shown in figure 4.

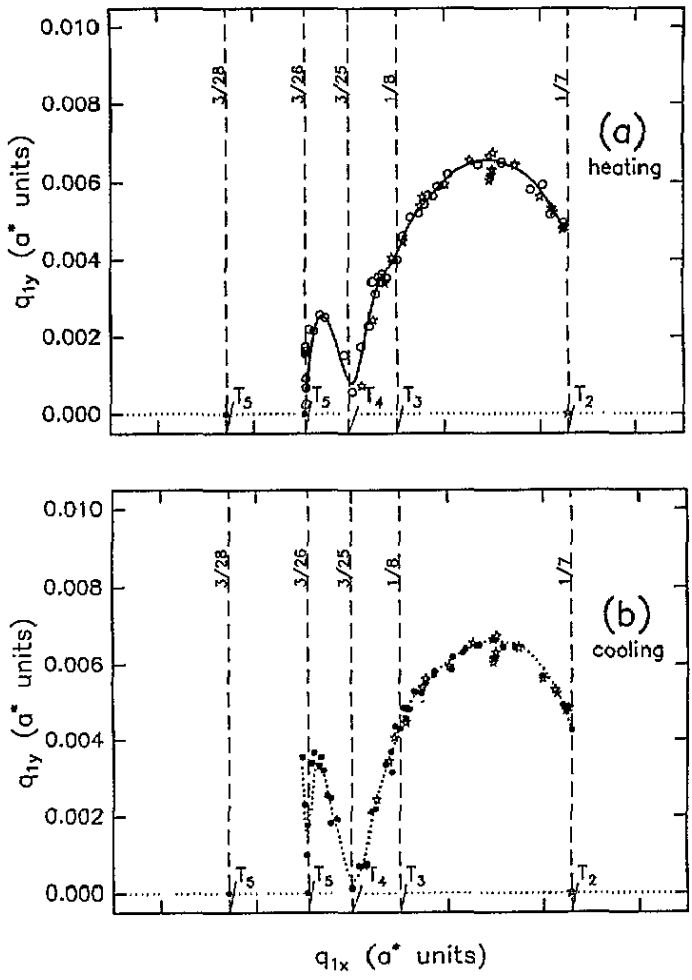


**Figure 8.** Basal plane components of the modulation vector describing the magnetic structure in pure Nd metal. The $q_{1y}$ component is shown as function of the $q_{1x}$ component in Nd metal. Temperature is an implicit parameter for both axes and $T_2$ corresponds to $(q_{1x}, q_{1y}) = (\frac{1}{7}, 0)$. The numbers against the dashed lines indicate the commensurate values of $q_{1x}$. The transition temperatures $T_N$ and $T_2$–$T_5$ correspond approximately to 19.3, 17.9, 10.5, 7.7 and 6.3 K on heating and to 19.1, 17.9, 8.7, 6.8 and 5.2 K on cooling. (a) and (b) correspond to heating and cooling, respectively. The solid curves are guides to the eye. The stars correspond to $(q_x, q_y)$ calculated for the higher-order commensurate magnetic structures described in section 4.

## 4. Discussion

Now let us consider figure 8 and first relate it to the ideas about commensurate–incommensurate transitions outlined in section 2. The figure has been constructed from the data in figure 7(b) and (c) (Risø data only) and shows $q_{1y}$ as function of $q_{1x}$ (or $q_{2x}$) with temperature as an implicit parameter. In fact, figure 8(a) shows the same data as reported by Lebech and Wolny (1992). At $T_N$ ($\sim$ 19.9 K), $q_1 = (q_{1x}, q_{1y}) \simeq (\frac{1}{7}, 0)$, and $q_1$ remains constant until $T_2$, approximately 1 K below $T_N$, where a second phase transition is observed (Lebech 1981, Zochowski and McEwen 1986). Below $T_2$, $q_{1x}$ decreases monotonically with temperatures and $q_{1y}$ becomes non-zero, i.e. the magnetic and the atomic structures are

incommensurate in one dimension. Within the framework of the description in section 2, the transition at $T_2$ may be considered to be a one-dimensional commensurate–incommensurate phase transition with order only on the hexagonal sites. However, according to previous experiments (McEwen *et al* 1985) and within the mean field approximation (Jensen and Mackintosh 1991), the transition at $T_2$ is also a transition from a single-$q$ structure to a two-$q$ structure. The small deviation from the commensurate value $\frac{1}{7}$ of the modulation vector observed at high temperatures between $T_N$ and $T_2$ does not cause any observable turn of $q$ away from the symmetry direction. A similar effect has been described by Shiba (1980) when considering epitaxial growth. Shiba (1980) explains this phenomena as being caused by weak interactions between adsorbed atoms, which are strongly coupled to the substrate. An analagous explanation may be feasible for the slight deviation from $\frac{1}{7}$ of the magnetic modulation vector in Nd.

In the incommensurate phase, (4) is no longer valid, but it becomes valid again when $q_y = 0$ once again after passing a maximum. We postulate that this happens at $T_3 \sim 10$ K, when $q_1 = (q_{1x}, q_{1y}) = (\sim \frac{1}{8}, 0)$ (see figure 7). At this temperature we observe kinks in the temperature dependences of both $q_{1x}$ and $q_{1y}$. From our present data we are not able to estimate whether there is any particular temperature at which (4) is exactly fulfilled for $n = 8$, and a new experiment on better single crystals is planned. As the temperature is lowered further to $\sim 8.2$ K a new set of magnetic Bragg peaks with a wave vector $q_3 = (q_{3x}, q_{3y}) = (\sim 0.187, 0)$ is observed (see figures 5 and 7). This additional magnetic ordering is ascribed primarily to ordered moments on the cubic sites. There are two experimental facts that should be noted: (i) the ratio between $|q_1|$ and $|q_3|$ at the transition is $\sim \frac{3}{2}$, i.e., when it first appears, $|q_3|$ is close to commensurate value $\frac{3}{16}$, and (ii), although $q_3$ is associated with order on the cubic sites, it is parallel to the direction of highest symmetry for the hexagonal sites. Therefore, below the transition at $\sim 8.2$ K, the interaction between cubic and hexagonal sites presumably becomes so strong that we may expect the commensurate values to be given by (6) rather than by (4). This is indeed in agreement with experiment. As the temperature is lowered further, $q_{1y}$ tends to zero for $q_{1x} = 1/(8 + \frac{1}{3}) = \frac{3}{25}$. There is considerable thermal hysteresis (see figure 7), and this behaviour occurs at different temperatures ($T_4$) on heating and cooling. Finally, at $T_5$ (also showing large thermal hysteresis, see figure 7) the next commensurate value of $q_1$ is observed. At this temperature $q_1$ splits into two satellites given by the commensurate values $q_1 = (1/(9-\frac{1}{3}), 0) = (\frac{3}{26}, 0)$ and $q_2 = (1/(9+\frac{1}{3}), 0) = (\frac{3}{28}, 0)$. Simultaneously, $q_3$ becomes incommensurate ($q_{3y} \neq 0$, see figures 5 and 7). Presumably at the same temperature, the fourth modulation $q_4$ appears, which in turn results in the fourfold splitting of the magnetic satellites corresponding to $q_{3x} = q_{4x} \sim 0.187$ and $q_{3y} \neq q_{4y}$ (see figure 5 (c)).

It should also be noted that, at 4.5 K in the proposed four-$q$ state, the lengths of the two commensurate modulation vectors $q_1$ and $q_2$ (Forgan *et al* 1989) agree reasonably well with (6), having $(q_{1x}, q_{1y}) = (1/(9 - \frac{1}{3}), 0) = (\frac{3}{26}, 0)$ and $(q_{2x}, q_{2y}) = (1/(9 + \frac{1}{3}), 0) = (\frac{3}{28}, 0)$, respectively. In contrast, the lengths of the incommensurate modulation vectors $|q_3| \sim |q_4|$ are slightly different from the commensurate value $1/(5 + \frac{1}{3}) = \frac{3}{16}$, and non-zero $q_{3y}$ and $q_{4y}$ components are indeed observed (see figure 5(c)). Additionally, it should be noted that as the interactions between the cubic and the hexagonal sites become stronger at low temperatures, we observe the splitting around a commensurate value into $q_1$ and $q_2$. This phenomenon can be explained if we assume that it arises because of the interaction between the cubic and the hexagonal sites. If the commensurate distance between the cubic sites in one layer and the hexagonal sites in the neighbouring layer below is equal to $(9 - \frac{1}{3})$, then the corresponding commensurate distance, between the same hexagonal sites and cubic site atoms in the neighbouring cubic layer below, is equal to $(9 + \frac{1}{3})$ (see also section 2 and

figure 1). The observation that the $q_3$ and $q_4$ modulation vectors become incommensurate when $q_1$ and $q_2$ become commensurate at low temperatures may be correlated to the fact that the direction of highest symmetry for hexagonal sites does not coincide with the direction of highest symmetry for cubic sites. Therefore the cubic satellites split in the perpendicular direction when the hexagonal becomes commensurate. However, deviations from the commensurate values $q_1 = (\frac{3}{26}, 0)$ and $q_2 = (\frac{3}{28}, 0)$ have been noticed below $T_5$. In order to illustrate this, we consider first the low-temperature hysteresis obtained when cooling to 4.2 K (figure 7(b)). Obviously, the transition to the $q_1 = (\frac{3}{26}, 0)$ and $q_2 = (\frac{3}{28}, 0)$ state shows pronounced hysteresis. Furthermore, when cooling from 13 K to 2.17 K and subsequently reheating to 13 K, another interesting behaviour appears. In this connection, the most relevant data for $q_1$ and $q_2$ are the eight left hand points in figure 7(b). On cooling from 13 K to 2.17 K the data points follow the dotted cooling curve to about 5.2 K, where $q_1 = (\frac{3}{26}, 0)$ and $q_2 = (\frac{3}{28}, 0)$ appear as expected from previous thermal cycling. Somewhere between 2.95 K and 2.17 K (cooling) $q_1$ and $q_2$ collapse into $q_1 \sim (\frac{1}{9}, 0)$, a state that persists at least up to 2.95 K when reheating. Above 13 K, the data follow the heating curves (figure 7, full curves). Unfortunately, no measurements were made between 2.95 K and 13 K on heating and the behaviour below 8.2 K of the magnetic structure and the modulation vectors is so complex that most of the above remarks about $q_1$, $q_2$, $q_3$ and $q_4$ need to be confirmed by future experiments on better single crystals.

In order to explain, at least phenomenologically, the temperature dependence of the modulation vector of the magnetic structure in Nd, we have pursued somewhat the ideas of commensurate magnetic structures outlined above and those of epitaxial growth (Shiba 1980, Grey and Bohr 1991, Bohr and Grey 1992). Our ideas are based on the experimental findings that, at some temperatures, the wave vector of the magnetic ordering in Nd seems to have a preference towards commensurate values such as $q = (\frac{1}{7}, 0)$, $(\frac{1}{8}, 0)$ etc as outlined above. We postulate that, within the experimental uncertainties, the modulation vectors, given by the solid and filled circles between $q = (\frac{1}{7}, 0)$ and $q = (\frac{1}{8}, 0)$ in figure 8, can also be represented by a special kind of higher-order commensurate structure in two dimensions, where the magnetic unit cell is turned around the hexagonal axis with respect to the crystallographic unit cell. The stars in figure 8 represent such structures. For $q_{1x} < \frac{1}{8}$, i.e. for $T < 10$ K, the $q$ dependence becomes more complex because of the interaction between the cubic and hexagonal site orderings and we will exclude attempts to explain the $q$ dependence below 10 K until the above postulate has been considered further theoretically and experimentally.

The postulate is based on the following idea. Within each hexagonal layer the Nd atoms lie on a regular lattice consisting of equilateral triangles with the sides of unit length. Equivalently, the spin system forms a fictive magnetic lattice, which may decorate the crystal lattice or 'grow epitaxially on it'. For a three-$q$ structure this fictive spin lattice consists also of equilateral triangles with sides whose length $(2\pi/|q|)$ differs from those forming the crystal lattice. Furthermore, for $q_y > 0$, the fictive spin lattice is turned through a small angle $\gamma$ with respect to the crystal lattice. Depending on the values of $|q|$ and $\gamma$, the fictive spin lattice may at some points coincide with points of the crystal lattice sites. This happens at lattice sites $r_l$, for which $q \cdot r_l = 2\pi$. In two dimensions, the magnetic structure is commensurate with the crystal lattice, but the commensurate cell is much larger than the original crystallographic cell. In general this higher-order commensurate magnetic unit cell is turned through an angle that may even be quite large with respect to the original crystallographic unit cell. We call this cell a higher-order commensurate cell. The length of the higher-order commensurate cell edge will not normally be commensurate with a suitably enlarged crystallographic unit cell. However, the magnetic

cell is commensurate in two dimensions, because in terms of hexagonal Miller indices the condition $h_C a_C + k_C b_C = h_S a_S + k_S b_S$ must be fulfilled. Here, $a_i$ and $b_i$ refer to the $a_1$ and $a_2$ hexagonal axes (figure 1) with $i$ = C or S, where C and S refer to the crystallographic cell and the magnetic (spin) unit cell. The misfit parameter $\alpha$ is given by

$$\alpha = |a_S|/|a_C| \tag{7}$$

and the rotation angle $\beta$ of the higher-order commensurate magnetic unit cell by

$$\tan(\beta) = k_C \sin(120°)/[h_C + k_C \cos(120°)]. \tag{8}$$

The idea is illustrated in figure 9. Figure 9(a) shows a three-$q$ magnetic lattice with $q = \langle \frac{1}{7}, 0 \rangle$ (unfilled circles) superimposed on the crystal lattice (filled circles). Not surprisingly the resulting commensurate magnetic cell (fine rhombus) is a $7 \times 7$ crystallographic unit cell (hexagonal units), which is larger than the normal crystallographic cell (small black rhombus in the left hand corner of figure 9(a)), but has the same orientation as this cell with respect to the crystallographic $a$- and $b$-axes. Figure 9(b) shows a similar pattern, but here the superimposed three-$q$ magnetic lattice is incommensurate with the crystal lattice and turned through a small angle $\gamma = \tan^{-1}(q_y/q_x)$ around the hexagonal axis with respect to the crystallographic cell. The crystal and spin lattices are commensurate in higher order in the way described above, and the resulting magnetic unit cell is turned through a rather large angle with respect to the crystal lattice and the crystallographic $a$- and $b$-axes. As in figure 9(a), the magnetic and the crystallographic cells are shown as fine and filled rhombuses, respectively. For illustrative purposes and in order to accommodate the magnetic unit cell within the lattice shown on the figures, the fine rhombuses show the mirror images of the cells defined by the Miller index axes $(h_C, k_C)$ and $(h_S, k_S)$ indicated in the lower left hand corners of figure 9(a) and (b). For the example shown in figure 9(b), $(h_C, k_C) = (24, 5)$ and $(h_S, k_S) = (25, 4)$ in hexagonal Miller indices with the misfit parameter $\alpha = 0.942\,92$ and the rotation angle $\beta = 11.387°$. In a more conventional notation, this corresponds to $q = \langle q_x, q_y \rangle = \langle 0.134\,70, 0.006\,64 \rangle$ in Cartesian coordinates or $|q| = 0.1349$ and $\gamma = 2.822°$ in polar coordinates.

The points shown by stars in figure 8(a) and (b) all represent magnetic higher-order commensurate lattices calculated similarly to the pattern shown in figure 9(b). One may therefore conclude that with decreasing temperature the magnetic structure of Nd goes through a series of two-dimensional commensurate–commensurate phase transitions rather than through a series of one-dimensional commensurate–incommensurate phase transitions. It should be remarked that, for illustrative purposes, figure 9 shows the situation for three-$q$ magnetic lattices. Single-$q$ and two-$q$ magnetic lattices will both form streaky patterns, because the triangles formed by the magnetic lattices consist of isosceles triangles instead of equilateral triangles. These types of lattice are also higher-order commensurate in the sense described above. However, the streaks formed by the single-$q$ and the two-$q$ lattices will be turned differently with respect to the $a$ and $b$-axes, because the isosceles triangles will have either two sides or one side of unit length. It is important to recognize that the stars shown in figure 8 do not in any way represent a unique set of higher-order commensurate magnetic lattices. In fact, there exist a discrete, but infinite number of higher-order commensurate lattices, which one might describe as a two-dimensional pattern of 'devil stairs'. The stars do, however, represent the particular set of magnetic lattices that agrees best with the experimental data in figure 8, and they have been chosen only to illustrate the postulate that the experimental points may indeed correspond to higher-order commensurate magnetic

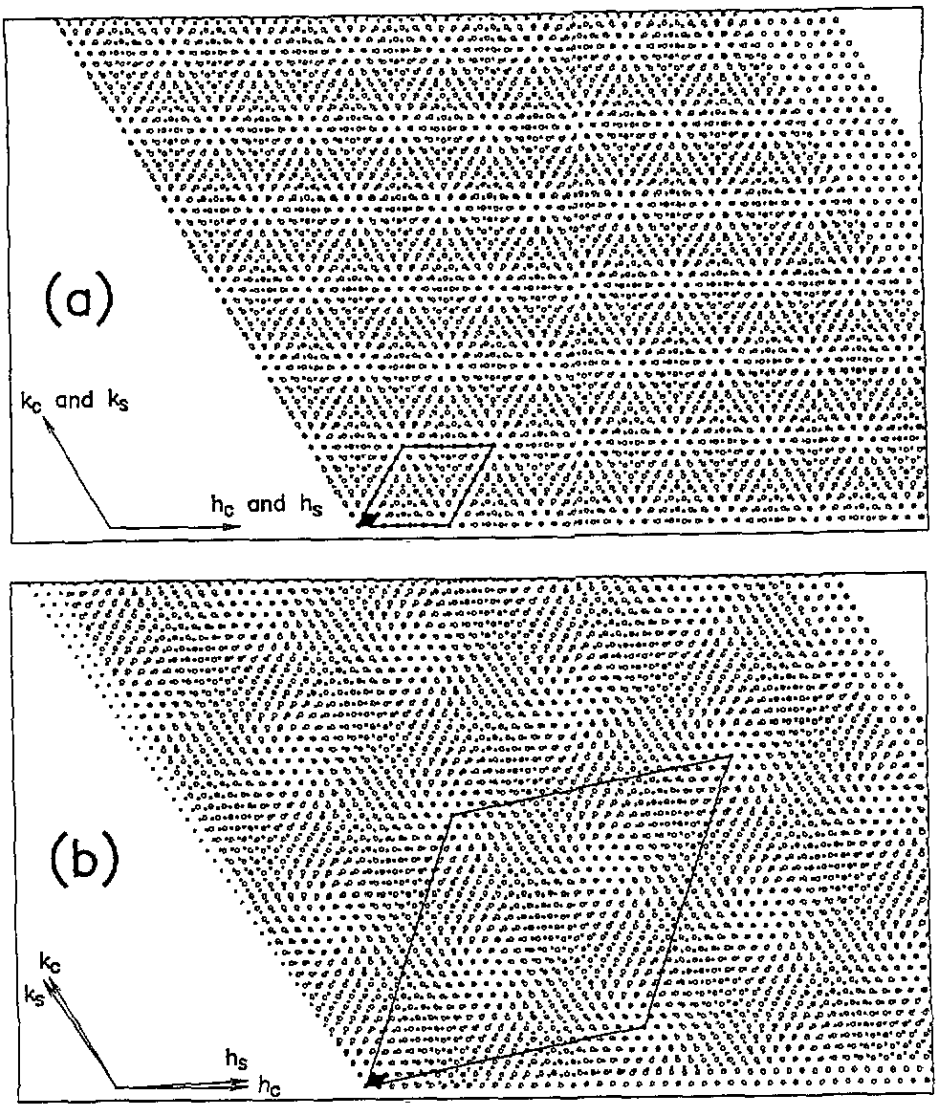


**Figure 9.** An illustration of the formation of the higher-order commensurate lattices, which may be obtained by rotating the fictive magnetic lattice (unfilled circles) through a small angle $\gamma$ with respect to the crystal lattice (filled circles). The cell of the crystal lattice is hexagonal with unit length. The magnetic lattices correspond to three-$q$ lattices with $q = (\frac{1}{7}, 0)$ (a) and $q \sim (0.1347, 0.0066)$ (b) (Cartesian coordinates). The crystallographic and the higher-order commensurate magnetic unit cells are shown by filled and fine rhombuses, respectively. It should be noted that in order to accommodate the magnetic unit cell within the lattice shown in these figures, the fine rhombuses show the mirror images of the cells defined by the Miller index axes $(h_C, k_C)$ and $(h_S, k_S)$. The relative directions of $(h_C, k_C)$ and $(h_S, k_S)$ are shown in the lower left hand corners of (a) and (b).

structures in Nd. In order to justify the postulate, it is necessary to calculate the free energy of the system and to consider theoretically the balance between for instance the magneto-elastic and anisotropy energies, which are some of the important mechanisms governing the temperature dependence of the magnetic modulation vector in Nd. We hope our experimental

findings will stimulate such efforts. It might also be added that recently Høgh Jensen (1994) made a theoretical study of the so called 'rotating staircase', a dynamic dissipative system with parameters $(q_x, q_y)$. This system was found to behave in a similar way as shown in figure 8, i.e. $q_y$ goes to zero whenever $q_x$ approaches a low rational number.

The ideas about two-dimensional commensurate magnetic structure in Nd naturally suggest a strong relationship between the crystal and the magnetic lattice. Presumably, the two lattices adjust to each other whenever the magnetic structure changes. Therefore, it would be informative to study the effects of the changes in magnetic structure on the lattice distortions by high-resolution synchrotron x-ray diffraction. In particular it would be feasible and of importance to study possible changes in lattice distortions at the transitions between the different multi-$q$ structures. Because the superimposed multi-$q$ magnetic and crystal lattices normally form streaky patterns of different orientations, it might even be possible to observe the change from a single-$q$ to a two-$q$ magnetic structure as a simple rotation of the crystallographic unit cell.

## Acknowledgments

We have benefited from stimulating discussions with J Bohr and M Høgh Jensen. Valuable comments from P Harris and S Aagaard Sørensen are also gratefully acknowledged.

## References

Bak P and Lebech B 1978 *Phys. Rev. Lett.* **40** 800
Bohr J and Grey F 1992 *Condens. Matter News* **1** 12
Forgan E M 1992 *J. Magn. Magn. Mater.* **104–107** 1485
Forgan E M, Gibbons E P, Lee S L, Zochowski S, McEwen K A and Marshall W G 1992a *J. Magn. Magn. Mater.* **104–107** 911
Forgan E M, Gibbons E P, McEwen K A and Fort D 1989 *Phys. Rev. Lett.* **62** 470
Forgan E M, Lee S L, Marshall W G and Fort D 1992b *J. Magn. Magn. Mater.* **104–107** 913
Gibbons E P, Forgan E M, Lee S L, McEwen K A, Marshall W G and Fort D 1992 *Physica* B **180 & 181** 91
Grey F and Bohr J 1991 *Phase Transitions in Surface Films 2* ed H Taub, G Torzo, H J Lauter and S C Fain (New York: Plenum) p 83
Høgh Jensen 1994 private communication
Jensen J and Mackintosh A R 1991 *Rare Earth Magnetism: Structures and Excitations* (Oxford: Clarendon) p 91
Koehler W C 1972 *Magnetic Properties of Rare Earth Metals* ed R J Elliott (New York: Plenum) p 81
Lebech B 1981 *J. Appl. Phys.* **52** 2019
Lebech B and Als-Nielsen J 1980 *J. Magn. Magn. Mater.* **15–18** 469
Lebech B, Als-Nielsen J and McEwen K A 1979 *Phys. Rev. Lett.* **43** 65
Lebech B and Nielsen M 1975 *RCN-234, Proc Neutron Diffraction Conf. 1975* (Petten) p 466
Lebech B and Wolny J 1992 *J. Magn. Magn. Mater.* **104–107** 1501
McEwen K A, Forgan E M, Stanley H B, Bouillot J and Fort D 1985 *Physica* B **130** 360
McEwen K A, Lebech B and Fort D 1986 *J. Magn. Magn. Mater.* **54–57** 457
McEwen K A, Lebech B and Vettier C 1982 *J. Magn. Magn. Mater.* **31–34** 171
McEwen K A and Stirling W G 1981 *J. Phys. C: Solid State Phys.* C **14** 157
Møller H B, Jensen J Z, Wulff M, Mackintosh A R, McMaster O D and Gschneidner K A Jr 1982 *Phys. Rev. Lett.* **49** 482
Moon R M, Cable J W and Koehler W C 1964 *J. Appl. Phys.* **35** 1041
Moon R M and Koehler W C 1980 *J. Magn. Magn. Mater.* **15–18** 503
Moon R M, Koehler W C, Sinha S K, Stassis C and Kline G R 1979 *Phys. Rev. Lett.* **43** 62
Novaco A D and McTague J P 1977 *Phys. Rev.* **38** 1286
Shiba H 1980 *J. Phys. Soc. Japan* **48** 211
Wolny J and Lebech B 1995 *J. Magn. Magn. Mater.* submitted

Zochowski S W, Marshall W G, McEwen K A, Fawcett E M, Forgan E M, Fort D and Shaik S 1992 *Physica* B **180–181** 26

Zochowski S W and McEwen K A 1986 *J. Magn. Magn. Mater.* 54–57 515

Zochowski S W, McEwen K A and Fawcett E 1991 *J. Phys.: Condens. Matter* 3 8079